Journal of Computational Biophysics and Chemistry

Research

Cite This: *J. Comput. Biophys. Chem.* **2023**, *22* (7), 829–843

A Multi-target Study of Natural Compounds in Preventing Neurodegenerative Disease Progression: A Computational Modeling Study

Yuri Alves de Oliveira Só, Mônica de Abreu Silva, Alessandra Sofia Kiametis and Camila D'Avila Braga Sette

Instituto de Física, Universidade de Brasília, Brasília, DF, Brazil

Marcelo Lopes Pereira Junior

Faculdade de Tecnologia, Departmento de Engenharia Elétrica, Universidade de Brasília, Brasília, DF, Brazil

Luiz Antônio Ribeiro Júnior and Ricardo Gargano*

Instituto de Física, Universidade de Brasília, Brasília, DF, Brazil

*Corresponding author. E-mail: *gargano@unb.br*

ABSTRACT: This work reveals how two natural multi-target compounds (Carnosine and Homocarnosine) can prevent the oligomerization of beta-amyloid peptides (Aβ). Properly combining molecular dynamics, docking and electronic structure calculations it was possible to investigate how Carnosine/Homocarnosine strongly interact with the amino acids of the Aβ(1-42) peptide responsible for the complexation with metallic ions (metallic hypothesis). This discovery may prevent the formation of harmful protein deposits, thereby preventing the progression of, for example, Alzheimer's disease (AD). These important results suggest that Carnosine/Homocarnosine can interact with, at least, two of the amino acids responsible for the complexation of the Aβ(1-42) peptide with the metallic ion copper(II). These findings open a new perspective on the inhibitory potential of these molecules in the treatment of AD and other neurodegenerative diseases.

KEYWORDS: Neurodegenerative disease; metallic and Aβ hypotheses; molecular dynamics; docking; carnosine and homocarnosine.

1. INTRODUCTION

Alzheimer's Disease (AD) is considered the most common cause of dementia among people over 60 years of age.[1] The number of people diagnosed with AD has been alarmingly increasing, according to a survey conducted in 2015, which accounted for 46.8 million people affected worldwide. This number is foreseen to double in the next 20 years.[2,3] Such a perspective is worrying, and several efforts have been made to treat the symptoms of AD or find a cure.

Aging is considered a risk factor for its onset.[4,5] The main signs of this disease are short- and long-term memory loss, cognitive delusions, disorientation, aggressive behavior and motor coordination impairment, which gradually worsen and can cause death.[6,7]

Several hypotheses seek to explain the origin of AD, and, to date, its cause is unknown. Among them are the cholinergic,[8] amyloid cascade,[9] Tau protein,[10] type 3 diabetes,[11] and metallic[12] hypotheses. Several biochemical and physical descriptors are found in AD patients, such as extracellular senile plaques formed by fibrillar aggre- gates of amyloid-beta (Aβ) peptides in brain regions and neurofibrillary tangles formed by the Tau protein.[3] Another common descriptor is the high concentrations of iron, zinc and copper metal ions.[13–15]

Received: 1 June 2023
Accepted: 18 July 2023
Published: 22 August 2023

World Scientific www.worldscientific.com © 2023 World Scientific Publishing Company

DOI: 10.1142/S2737416523500436
J. Comput. Biophys. Chem. **2023**, *22* (7), 829–843

Some studies[16–19] suggest that the oligomerization of peptides from Aβ(1–42) is accelerated through the interaction of the copper(II) metal ion with the aspartate 1, alanine 2 and histidines 6 or 13/14 amino acids. The interaction with this metal, according to the metallic hypothesis, is indicated as responsible for the accelerated process of oligomerization of Aβ(1–42) peptides and the consequent formation of amyloid plaques. Based on the metallic hypothesis, we conducted a study to investigate the stability of Carnosine complexes with copper and zinc metallic ions, using proposed conformations from the previous literature.[17,18,20,21] Additionally, we investigated the potential of the Carnosine and one of the derivates, Homocarnosine, in preventing the progression of Alzheimer's disease (AD). To accomplish this, we considered the tautomeric forms of the compounds and performed calculations to determine their ability to prevent interactions between the Aβ(1–42) peptide and copper(II) metal ions. Our computational protocol involved a multi-target interaction study of these compounds with metallic ions and Aβ(1–42) peptides, utilizing *ab initio* calculations to prevent peptide aggregation.

1.1. Carnosine and homocarnosine natural molecules

Carnosine (CA) in Fig. 1, is a naturally occurring dipeptide consisting of β-alanine and L-histidine. Its functions are calcium regulator, antioxidant, metal ion toxicity reduction, an inhibitor of Advanced Glycoxidation End-products (AGEs) and Advanced Lipoxidation End-products (ALEs), among others.[22] It has been proposed as a therapeutic agent for many diseases, including cancers, neurodegenerative diseases, diabetes, and schizophrenia.[23,24] However, due to its low concentration in some body regions, its action may be limited.[25]

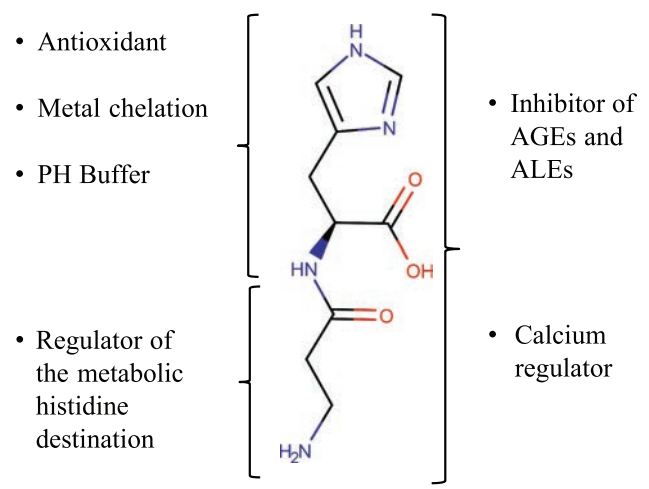

Fig. 1. (Color Online) Representation of the structure–activity relationship of Carnosine: The imidazole ring is required for antioxidant, metal ion chelating and buffering activity. The β-alanine structure regulates the metabolic destination of the L-histidine residue and the synthesis of Carnosine. Both β-alanine and L-histidine act synergistically to inhibit the formation of AGEs and ALEs.

The majority of Carnosine (in the range of one millimolar) is produced in the muscular tissues of the bones and in the olfactory bulb. They concentrate about 99% of the bioavailability in the organism, with a minor concentration found in the brain region and other tissues of the body (from ten to thousand times smaller than in muscles). It has a lifespan of fewer than five minutes in the human body, rapidly cleaving into β-alanine and L-histidine by hydrolytic Carnosinase enzymes. With advancing age, more hydrolytic carnosinases are produced by the human body, consequently decreasing the amount of Carnosine in the body. Therefore, there is a need to synthesize and analyze new substances.[25–27]

Carnosine has some natural derivatives that perform similar bodily functions, such as Anserine, Ophidine and Homocarnosine. Carnosine is the most common form in humans, Anserine is typically found in birds and rodents and Ophidine is most often found in whales, dolphins and snakes. Among them, the most common form is Homocarnosine (HCA), γ-aminobutyric-L-histidine, probably due to the greater availability of the components that compose it, such as the more significant presence of γ-aminobutyric acid in the central nervous system. Its concentration in the brain is about one millimolar, comparable to the concentration of Carnosine found in muscle tissue.[25,28,29]

Carnosine and Homocarnosine are made up of an L-histidine structure. The difference between them concerns the rest of the structure, where the first is composed of a γ-alanine, and the second one of a γ-aminobutyric acid (GABA), as shown in Fig. 2.

Carnosine can activate brain function by overcoming the blood-brain barrier (BBB), reaching the central nervous system and activating glial cells. These cells secrete neurotrophins, activating neuronal cells indirectly in response to Carnosine. Carnosine-activated glial cells can support the elimination of Aβ species and trigger the repair of damaged neurons during AD. This ability may be necessary for treating AD since neurotoxic Aβ species that accumulate in the brain of patients can result in dysregulation of proinflammatory cytokine production. Furthermore, it is reported

DOI: 10.1142/S2737416523500436
J. Comput. Biophys. Chem. **2023**, *22* (7), 829–843

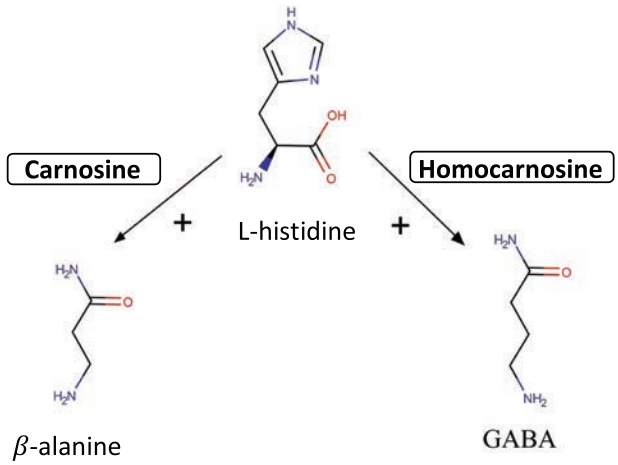

Fig. 2. (Color Online) Schematic representation of the structural differences between Carnosine and Homocarnosine.

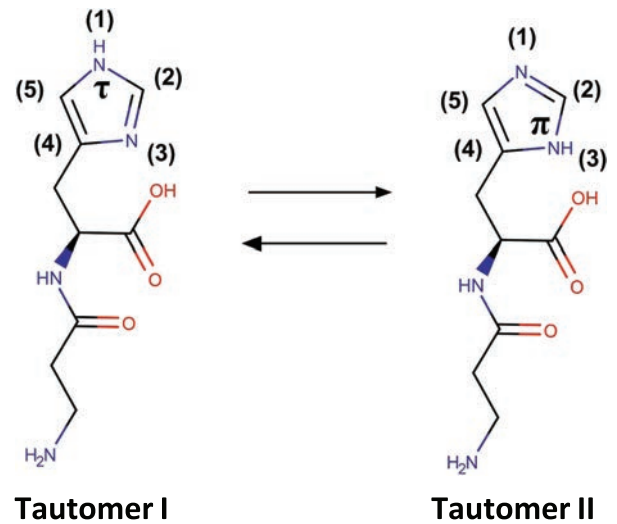

Fig. 3. (Color Online) Tautomeric forms of the imidazole ring of Carnosine.

that Carnosine has antioxidant and chelating properties of metal ions, such as copper(II), zinc(II) and nickel(II), which are predicted to be responsible for the oligomerization of Aβ peptides and, consequently, damage to brain functions, according to the metallic AD hypothesis. In this way, Carnosine and its derivatives may contribute to avoiding or mitigating some of the damages resulting from AD.[25,30]

The two tautomeric forms of the imidazole ring of Carnosine in its neutral form are the protonated N_τ (tautomer I) at position 1 and the protonated N_π (tautomer II) at position 3, shown in Fig. 3. Studies in Raman spectroscopy indicate that both tautomers exist at neutral pH, thus indicating an equilibrium between the two tautomeric forms.

Furthermore, at pH 7–9, tautomer I is the most predominant species (75%), with tautomer II being less energetically stable than tautomer I. However, this tautomeric balance can be affected by the chelation of metals, prevailing in this situation, tautomer II.[25]

2. METHODS

2.1. *Ab initio* calculations

In the literature, there are several proposals for copper[31–34] and zinc[35] Carnosine complexes. To investigate the interaction of Carnosine with metallic ions and the stability of the proposed complexes, three complexes of copper and four complexes with zinc, we perform geometry optimization and frequency calculations for each complex using Density Functional Theory (DFT) at the (U)B3P86/6-311+G(*d*,*p*) level for C, N, O and H atoms and with LANL2DZ ECP for copper and zinc. To account for solvation effects, we also used the Polarizable Continuum Model (PCM) with water as a solvent to calculate the Gibbs free energy at 298.15 K. The methods used in this study are based on the work of Trouilhas *et al.*,[36] who determined that the (U)B3P86/6-311+G(*d*,*p*) method is the most suitable for calculating antioxidant properties of phenolic compounds.

2.2. NCI analysis

NonCovalent Interactions (NCIs) are powerful methods that allow for the detection and visualization of various NCIs such as hydrogen bonds, steric clashes and van der Waals interactions.[37–39] The techniques use the density and its derivatives to generate an index called the Reduced Density Gradient (RDG). This index is calculated using the density and its first derivative:

$$s(\rho) = \frac{1 - |\nabla\rho|}{2(3\pi^2)^{1/3}\rho^{1/3}}.$$

When weak inter- or intramolecular interactions are present, the reduced gradient between the interacting atoms undergoes a significant change, which leads to the appearance of density critical points between the interacting fragments. Troughs are observed in $s(\rho)$ that are associated with each critical point. However, the behavior of s at low densities is mostly governed by ρ, so s tends to diverge except in the regions around a density critical point, where $\nabla\rho$ dominates and s

DOI: 10.1142/S2737416523500436
J. Comput. Biophys. Chem. **2023**, *22* (7), 829–843

approaches zero.[40] From the NCI analysis, which uses the electron density function to identify attractive and repulsive interactions between atoms, we can produce a RDG scatter plots, which are a graphical representation of the electron density and the strength of the attractive or repulsive interactions between atoms in a molecular system.[41] The axis RDG represents the electron density of the molecular system and the axis sign(λ_2)ρ represents the stability of the molecular system. It is a combination of the second smallest eigenvalue of the electron density Hessian matrix (λ_2) and the electron density (ρ). The sign (λ_2)ρ is used to identify regions of the molecular system where attractive interactions are particularly stable, regions with high values, more negative, indicate that the attractive interactions are stable and contribute significantly to the overall stability of the system.[42] This method can provide valuable insights into molecular interactions and their mechanisms.

2.3. Molecular docking

To investigate the interaction between ligands and the peptide Aβ, we first determined the regions with the highest probability of interaction between a monomer of Aβ(1–42) and Carnosine N_τ ($CA_{N\tau}$), Carnosine N_π ($CA_{N\pi}$), Homocarnosine N_τ ($HCA_{N\tau}$) and Homocarnosine N_π ($HCA_{N\pi}$). This mapping was necessary to verify if these ligands can interact with the same amino acids that interact with copper(II) in the complexation with the Aβ(1–42) peptide. Based on that, the molecular docking of Carnosine and Homocarnosine was performed with 10 conformations selected from a set of 1880 conformations obtained by Sette *et al.*[43] from molecular dynamics calculations with 211 ns of total simulation, selecting for each docking calculation the 10 lowest energy complexes. This was done to take into account the different conformations that the Aβ(1–42) protein can assume so that the 10 best poses of the ligands, for each of the 10 conformations of the protein. With this procedure, a total of 100 different poses were obtained for each ligand. To obtain the binding sites between the ligands (Carnosine and Homocarnosine) and the Aβ(1–42) peptide, molecular docking was performed considering the entire Aβ(1–42) protein.

We used the AutoDock 4.2[44] program to perform molecular docking simulations.

The ligands and the macromolecule were prepared by employing Gasteiger's partial charge method[45] based on empirical calculations of electronegativity equilibrium. The docking protocol considers a 60 × 60 × 60 grid with a spacing of 1.0 ˚Å. The macromolecule was kept rigid, and the ligand was free to rotate the active bonds. The docking procedure includes the Lamarckian genetic algorithm.[46] This algorithm generates conformations through a stochastic process with three ligand degrees of freedom: Translational, rotational and conformational. The conformations vary randomly in each run, using the following parameters: 100, 150 and 250,00,000 for the number of conformations (runs), number of initial conformations (population) and maximum long energy ratings, respectively.

Through LigPlot+,[47] we automatically generate 2D ligand–protein interaction diagrams from 3D coordinates in PDB format. These diagrams help identify patterns of hydrogen bonds and hydrophobic interactions between ligand–protein complexes. Generally speaking, a hydrogen bond is an attractive interaction between two electronegative atoms, where one is the donor and the other the acceptor of electrons. A hydrogen atom is aligned between them and covalently bonded to the donor. The donor atom attracts the hydrogen electron from its orbital towards the donor atom itself, which causes a partial positive charge on the hydrogen, which is electrostatically attracted to the electronegative acceptor atom.

Qualitatively, the hydrophobic interaction causes hydrophobic parts to aggregate or cluster in polar media. This trend occurs due to the dynamic actions of nonpolar compounds in the environment that interact with each other and force the interaction of nonpolar compounds. LigPlot+ identifies bonds and interactions according to the criteria of distance and angle between the ligand and receptor atoms.[48,49]

One of the parameters obtained by the AutoDock 4.2 program and used to perform the analysis is the score function, which corresponds, in this case, to the binding energy or Gibbs free energy (ΔG). It is a measure of the binding affinity of the ligand–receptor complex, given by the difference between the energy of the complex and the sum of the energies of the ligand and the receptor separately.

3. RESULTS AND DISCUSSION

3.1. Evaluation of conformations of CA/Cu^{2+} and CA/Zn^{2+} complexes

The systems selected for this study were three copper complexes previously proposed in the literature by Dobbie and Kermack,[50] Martin and Edsall[32] and Ihnat and Bersohn,[34] respectively named CA/Cu^{2+}-I, CA/Cu^{2+}-II and CA/Cu^{2+}-III. For the zinc complexes, we selected four complexes that were previously proposed

DOI: 10.1142/S2737416523500436
J. Comput. Biophys. Chem. **2023**, *22* (7), 829–843

by Matsukura *et al.*[51] The zinc complexes were similarly designed as the copper complexes, with a numbering system of I–IV.

Figures S1 and S2 depict the optimized conformations of CA/Cu^{2+} and CA/Zn^{2+} complexes, and Table S1 lists the distances between the metallic ions and the atoms they interact with, along with the predicted geometry from our calculations. The vibrational spectra of the geometrically optimized molecules showed no imaginary frequencies, indicating that they were at the global minimum of their potential energy surfaces. We found that the CA/Cu^{2+}-I/II complexes were trigonal pyramidal, while the CA/Zn^{2+}-I/II complexes were trigonal bipyramidal and the CA/Cu^{2+}-III and CA/Zn^{2+}-III/IV complexes were square planar. Our results show that CA/Cu^{2+}-III had the shortest distances from the metallic ion among the copper complexes, whereas CA/Zn^{2+}-II/IV had the shortest distances among the zinc complexes.

The calculated Gibbs free energy values for the studied complexes, presented in Table 1, show significant differences between the copper complexes, with CA/Cu^{2+}-III having the most negative value (–106.22 Kcal/mol) and CA/Cu^{2+}-I having the least negative value (–67.95 Kcal/mol). This suggests that the stability of these complexes increases as we move from CA/Cu^{2+}-I to CA/Cu^{2+}-III, indicating that the formation of CA/Cu^{2+}-III complex is favored thermodynamically. For the zinc complexes, the results indicate that there are small differences in the thermodynamic stability of these complexes. The CA/Zn^{2+}- II complex has the least negative Gibbs free energy value (–96.67 Kcal/mol), followed closely by CA/Zn^{2+}-I (–97.68 Kcal/mol). In contrast, the CA/Zn^{2+}-III and CA/Zn^{2+}-IV complexes have the most negative Gibbs free energy values (–102.24 Kcal/mol and –102.96 Kcal/mol, respectively).

We conducted an NCI analysis to investigate the interactions between the ligand and metallic ion, and found that specific atom–atom interactions play a key role. Our results suggest that the metallic ions Cu^{2+} and Zn^{2+} interact mainly through attractive and steric interactions with the ligand. In Fig. 4, we can see that CA/Cu^{2+}-I and CA/Cu^{2+}-III have the strongest interactions with copper, while CA/Cu^{2+}-II shows a minor repulsive and attraction interaction. The results also show that CA/Cu^{2+}-III presents a minor re pulsive interaction in the vicinity of the metallic ion that the CA/Cu^{2+}-I. In Fig. 5, we observe from the spikes that CA/Zn^{2+}-I has weaker steric interactions but stronger attractive interactions with the metallic ion, while CA/Zn^{2+}-II, CA/Zn^{2+}-III and CA/Zn^{2+}-IV show stronger steric interactions. We can also observe from the spikes that the CA/Zn^{2+}-I presented van der Waals interactions more pronounced than the other complexes.

Combining the results of the study shows that the most stable copper complex is CA/Cu^{2+}-III which was proposed by Ihnat and Bersohn.[34] This complex exhibits a smaller distance between the copper ion and the atom donors of the Carnosine, as well as a smaller Gibbs free energy value. Additionally, this complex has a lower steric interaction and a higher attractive interaction compared to the other copper complexes studied. The observed trend in the Gibbs free energy values can be attributed to the differences in the structure and coordination of the copper ion within each complex, which can affect the energy required to form the complex. For complexes of copper with Carnosine, the geometry square planar must be preferred without the participation of the Carnosine ring in the interaction with the copper ion. Regarding the zinc complexes, CA/Zn^{2+}-I is predicted to be the most stable, with Gibbs free energy values comparable to CA/Zn^{2+}-II,

Table 1. Gibbs free energy of metallic the complexes of Carnosine with $Cu2^{+}$ and $Zn2^{+}$ calculate at level UB3P86 and basis set 6-311+G(*d*,*p*)/LANL2DZ ECP with PCM model (solvent: water).

Complex	$E_{Complex}$ (Hartree)	E_{Ligand} (Hartree)	E_{Metal} (Hartree)	E_{Water} (Hartree)	ΔG (Hartree)	ΔG (Kcal/mol)
CA/Cu^{2+}-I	–1070.299587	–796.982613	–196.569469	–76.639221	–0.1083	–67.95
CA/Cu^{2+}-II	–1070.334954	–796.982613	–196.569469	–76.639221	–0.1437	–90.14
CA/Cu^{2+}-III	–1070.360575	–796.982613	–196.569469	–76.639221	–0.1693	–106.22
CA/Zn^{2+}-I	–939.638352	–796.982613	–65.860855	–76.639221	–0.1557	–97.68
CA/Zn^{2+}-II	–939.636735	–796.982613	–65.860855	–76.639221	–0.1540	–96.67
CA/Zn^{2+}-III	–939.645615	–796.982613	–65.860855	–76.639221	–0.1629	–102.24
CA/Zn^{2+}-IV	–939.646772	–796.982613	–65.860855	–76.639221	–0.1641	–102.96

DOI: 10.1142/S2737416523500436
J. Comput. Biophys. Chem. **2023**, *22* (7), 829–843

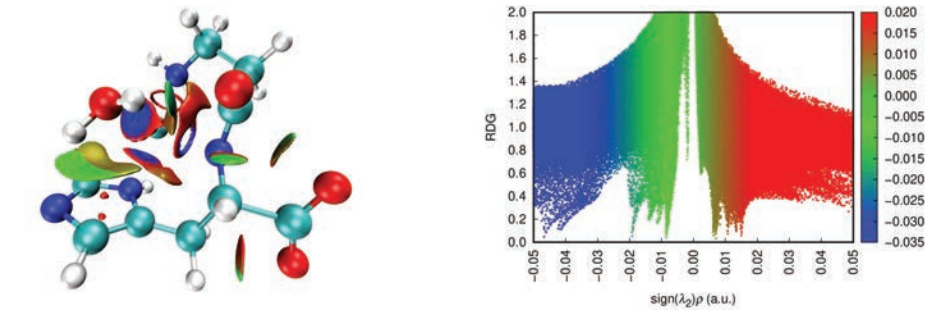

(a) CA/Cu^{2+}-I

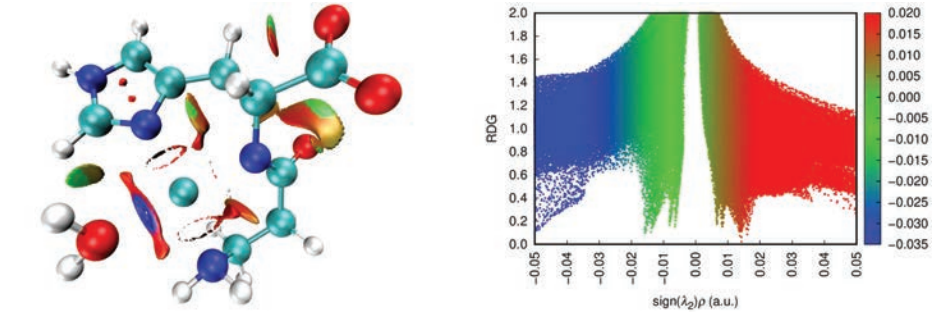

(b) CA/Cu^{2+}-II

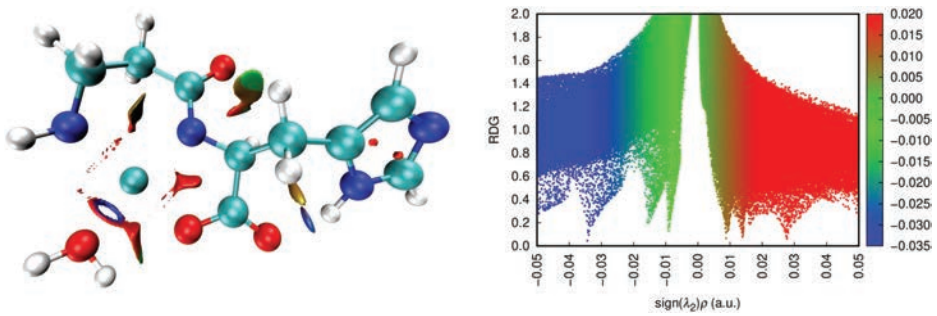

(c) CA/Cu^{2+}-III

Fig. 4. (Color Online) NCI surfaces (left) and RDG scatter plots (right). Color scheme: Blue represents strong attractive interactions, green indicates van der Waals interactions and red indicates repulsive/steric interactions. In the RDG scatter plots, from zero, how much more to the right stronger the attraction, more to the left more strong the repulsion.

but with more attractive and van der Waals interactions compared to the other complexes studied. However, given the proximity of the results, both I and II may be possible complexes with zinc, with geometry trigonal bipyramidal being preferred and with or without the participation of the Carnosine ring in the interaction with the zinc ion.

3.2. Carnosines and Aβ interaction

We begin our discussion by presenting in Table 2 and Fig. 6 energy weight results for the $CA_{N\tau}/A\beta(1–42)_i$ (ligand/protein) interaction, where i is the index that represents one of the 10 conformations selected from the molecular dynamics. Tables S2 and S3 in the Supplementary Material present their related ΔG energies, used to define the energy weight calculated for each type of interaction (hydrogen bonds and hydrophobic contacts). The energy weight value is the total sum of ΔG values for each amino acid interaction in the ligand/protein complex. We considered the 10 lowest energy complexes of 10 ligand/peptide conformations.

As a general trend, the 10 lowest energies of each amino acid vary approximately 1 Kcal/mol between them, indicating that these complexes are equally likely. For all the complexes, the $A\beta(1–42)_1$ has the lowest energy. Moreover, the energy differences are less than 3 Kcal/mol for $A\beta(1–42)_6$, 2 Kcal/mol for $A\beta(1–42)_2$ and $A\beta(1–42)_9$ and 1 Kcal/mol for the other complexes. Furthermore, among the remaining complexes, the ligand/peptide complexes from $A\beta(1–42)_3$ to $A\beta(1–42)_8$

DOI: 10.1142/S2737416523500436
J. Comput. Biophys. Chem. **2023**, *22* (7), 829–843

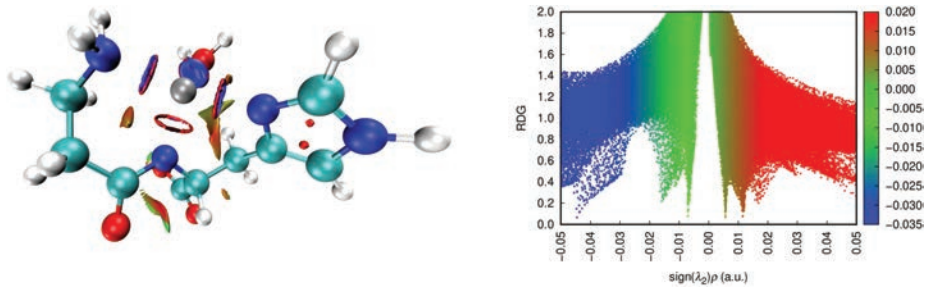

(a) CA/Zn^{2+}-I

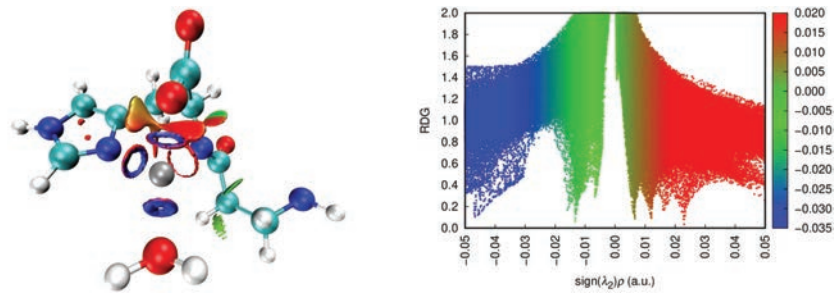

(b) CA/Zn^{2+}-II

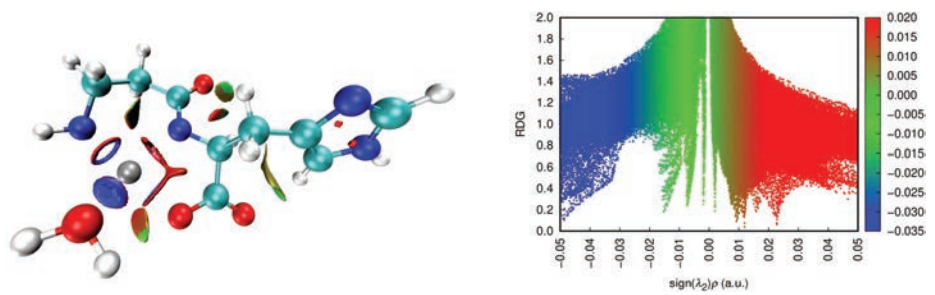

(c) CA/Zn^{2+}-III

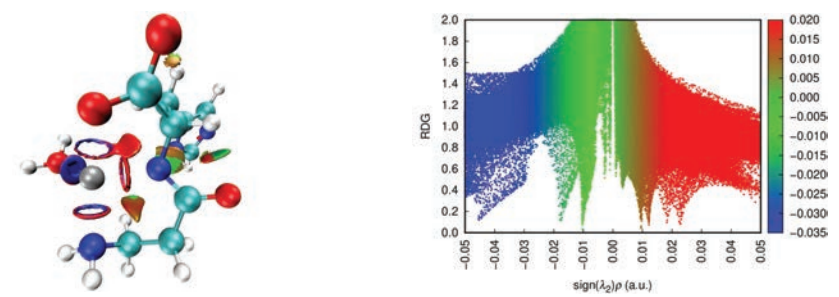

(d) CA/Zn^{2+}-IV

Fig. 5. (Color online) NCI surfaces (left) and RDG scatter plots (right). Color scheme: Blue represents strong attractive interactions, green indicates van der Waals interactions and red indicates repulsive/steric interactions. In the RDG scatter plots: From the zero, how much more to the right stronger the attraction, more to the left more strong the repulsion.

and the A$\beta(1–42)_{10}$ have similar energies. The constant inhibition (K_i) values, presented in Table S1, have the same trend of the energies and can also be used to rank the most likely conformations. The K_i indicates the stability of the complex, representing the ligand's efficacy in inhibiting the receptor and the amount of drug needed to carry out the inhibition. The lower the K_i value, the greater the stability of the complex.

Considering the interaction site of copper(II) with Aβ(1–42), predicted by the literature,[16–19] $CA_{N\tau}$ interacts with at least two amino acids responsible for aggregating Aβ(1–42) peptide with the metal ion: the Asp1 (by hydrophobic contact) and the Hsd13 (by hydrogen bond and hydrophobic contact). The results presented in Table 2 and Fig. 6 suggest that $CA_{N\tau}$ interacts with Aβ(1–42) by hydrogen bond, mainly with the

DOI: 10.1142/S2737416523500436
J. Comput. Biophys. Chem. **2023**, *22* (7), 829–843

Table 2. Energy weight percentages for each amino acid interaction (hydrogen bonds and hydrophobic contacts) in the $CA_{N\tau}$/Aβ(1–42) complexes obtained using molecular docking. We considered the 10 lowest energy complexes of 10 ligand/peptide conformations.

		Energy weight (Hydrogen bond)		Energy weight (Hydrophobic contact)	
Amino acid	Abbreviation	Kcal/mol	%	Kcal/mol	%
Aspartate	Asp1	–33.90	4.23	–30.02	5.31
Alanine	Ala2	–8.91	1.11	–26.54	4.69
Glutamate	Glu3	–53.56	6.69	–23.09	4.08
Phenylalanine	Phe4	–43.25	5.40	–86.80	15.34
Arginine	Arg5	–83.34	10.41	–13.59	2.40
Histidine	Hsd6	–21.02	2.62	–17.65	3.12
Aspartate	Asp7	–64.46	8.05	0.00	0.00
Serine	Ser8	–11.36	1.42	–11.67	2.06
Glycine	Gly9	–13.69	1.71	–4.88	0.86
Tyrosine	Tyr10	–4.80	0.60	–2.23	0.39
Glutamate	Glu11	–21.69	2.71	–4.80	0.85
Valine	Val12	–2.23	0.28	–41.32	7.30
Histidine	Hsd13	–69.70	8.70	–30.59	5.41
Histidine	Hsd14	–3.36	0.42	–22.94	4.05
Glutamine	Gln15	–41.70	5.21	–21.59	3.82
Lysine	Lys16	–50.36	6.29	–24.22	4.28
Leucine	Leu17	–77.58	9.69	–18.44	3.26
Valine	Val18	0.00	0.00	–1.92	0.34
Phenylalanine	Phe19	–6.05	0.76	–71.50	12.64
Phenylalanine	Phe20	–2.11	0.26	–13.69	2.42
Alanine	Ala21	–11.00	1.37	0.00	0.00
Glutamate	Glu22	–2.11	0.26	0.00	0.00
Aspartate	Asp23	–18.68	2.33	–10.66	1.88
Valine	Val24	–7.59	0.95	–2.58	0.46
Glycine	Gly25	–18.40	2.30	–10.00	1.77
Serine	Ser26	–19.67	2.46	–12.83	2.27
Asparagine	Asn27	–37.03	4.62	–2.53	0.45
Lysine	Lys28	–35.00	4.37	–4.65	0.82
Glycine	Gly29	–9.26	1.16	–2.30	0.41
Alanine	Ala30	0.00	0.00	0.00	0.00
Isoleucine	Ile31	0.00	0.00	–9.74	1.72
Isoleucine	Ile32	0.00	0.00	0.00	0.00
Glycine	Gly33	0.00	0.00	0.00	0.00
Leucine	Leu34	0.00	0.00	0.00	0.00
Methionine	Met35	0.00	0.00	0.00	0.00
Valine	Val36	0.00	0.00	–2.60	0.46
Glycine	Gly37	–10.26	1.28	0.00	0.00
Glycine	Gly38	0.00	0.00	–5.05	0.89
Valine	Val39	–4.87	0.61	–9.45	1.67
Valine	Val40	–7.22	0.90	–9.26	1.64
Isoleucine	Ile41	–4.27	0.53	–7.36	1.30
Alanine	Ala42	–2.48	0.31	–9.31	1.65
Total energy weight		–800.91	—	–565.80	—

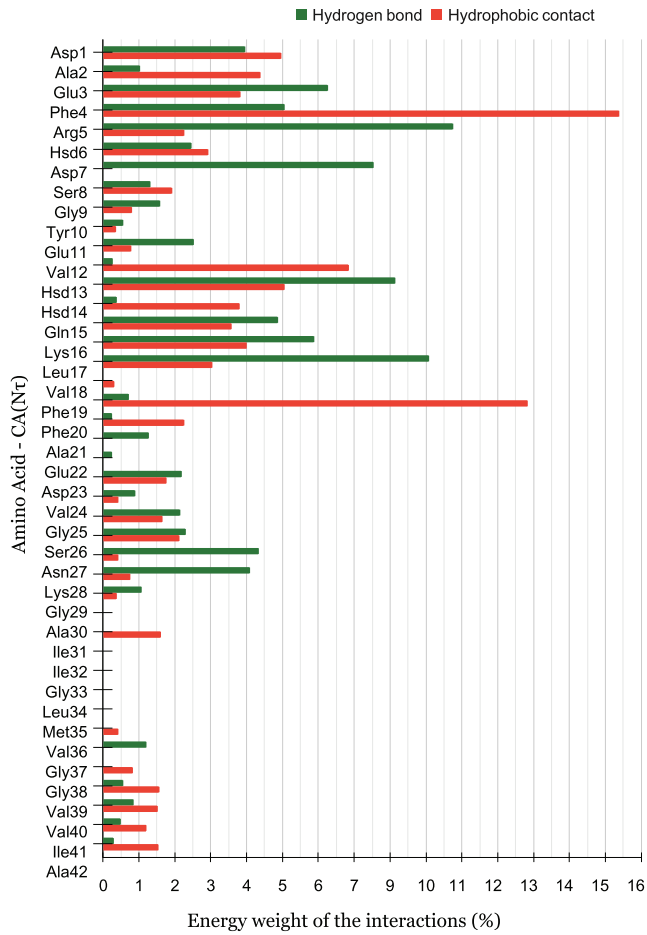

Fig. 6. (Color online) Energy weight percentages for the amino acid interactions (hydrogen bonds and hydrophobic contacts) in the $CA_{N\tau}$/Aβ(1–42) complexes. We considered the 10 lowest energy complexes of 10 ligand/peptide conformations.

following amino acids: Arg5 (10.41%), Leu17 (9.69%), Hsd13 (8.70%), Asp7 (8.05%) and Glu3 (6.69%). By hydrophobic contact, the main interactions are the ones with amino acids Phe4 (15.34%), Phe19 (12.64%), Val12 (7.30%), Hsd13 (5.41%) and Asp1 (5.31%).

ΔG energy results for $CA_{N\pi}$/A$\beta(1–42)_i$ interaction are shown in Supplementary Material (see Tables S4 and S5). From these results, the energy weights were calculated (hydrogen bond and hydrophobic contacts) and the results are presented in Table 3 and Fig. 7.

The results also show that the 10 lowest energies of each complex vary by 1 Kcal/mol, indicating that these complexes are likely equal. For all the complexes, A$\beta(1–42)_1$ has the lowest energy and presents an energy difference of about 1.5 Kcal/mol smaller than the other complexes. The complex with A$\beta(1–42)_9$ showed an energy difference of 1 Kcal/mol. The remaining complexes, from A$\beta(1–42)_2$ to A$\beta(1–42)_8$ and the A$\beta(1–42)_{10}$ have similar energies. According to

DOI: 10.1142/S2737416523500436
J. Comput. Biophys. Chem. **2023**, *22* (7), 829–843

Table 3. Energy weight percentages for each amino acid interaction (hydrogen bonds and hydrophobic contacts) in the $CA_{N\pi}$/Aβ(1–42) complexes obtained using molecular docking. We considered the 10 lowest energy complexes of 10 ligand/peptide conformations.

		Energy weight (Hydrogen bond)		Energy weight (Hydrophobic contact)	
Amino acid	Abbreviation	Kcal/mol	%	Kcal/mol	%
Aspartate	Asp1	−32.84	5.58	−6.33	1.25
Alanine	Ala2	−22.41	3.81	−6.49	1.28
Glutamate	Glu3	−52.42	8.90	−1.93	0.38
Phenylalanine	Fene4	−26.69	4.53	−58.61	11.57
Arginine	Arg5	−50.93	8.65	−35.56	7.02
Histidine	Hsd6	−28.57	4.85	−63.25	12.49
Aspartate	Asp7	−50.62	8.60	0.00	0.00
Serine	Ser8	−25.47	4.33	0.00	0.00
Glycine	Gly9	−4.33	0.74	−8.62	1.70
Tyrosine	Tyr10	−4.46	0.76	−18.18	3.59
Glutamate	Glu11	−38.80	6.59	−7.96	1.57
Valine	Val12	−2.65	0.45	−55.99	11.05
Histidine	Hsd13	−43.04	7.31	−29.48	5.82
Histidine	Hsd14	−6.96	1.18	−6.06	1.20
Glutamine	Gln15	−21.74	3.69	−32.03	6.32
Lysine	Lys16	−14.51	2.46	−36.43	7.19
Leucine	Leu17	−28.86	4.90	−21.40	4.22
Valine	Val18	0.00	0.00	−12.13	2.39
Phenylalanine	Phe19	−1.97	0.33	−47.64	9.40
Phenylalanine	Phe20	−4.87	0.83	−3.47	0.68
Alanine	Ala21	−1.97	0.33	0.00	0.00
Glutamate	Glu22	−11.65	1.98	0.00	0.00
Aspartate	Asp23	−11.08	1.88	−2.13	0.42
Valine	Val24	0.00	0.00	0.00	0.00
Glycine	Gly25	−9.30	1.58	0.00	0.00
Serine	Ser26	−15.30	2.60	−1.85	0.37
Asparagine	Asn27	−22.46	3.81	−11.58	2.29
Lysine	Lys28	−26.16	4.44	−4.86	0.96
Glycine	Gly29	−6.78	1.15	−7.94	1.57
Alanine	Ala30	0.00	0.00	0.00	0.00
Isoleucine	Ile31	−1.85	0.31	0.00	0.00
Isoleucine	Ile32	0.00	0.00	0.00	0.00
Glycine	Gly33	0.00	0.00	0.00	0.00
Leucine	Leu34	0.00	0.00	0.00	0.00
Methionine	Met35	0.00	0.00	0.00	0.00
Valine	Val36	0.00	0.00	0.00	0.00
Glycine	Gly37	−1.85	0.31	0.00	0.00
Glycine	Gly38	−1.85	0.31	0.00	0.00
Valine	Val39	−1.52	0.26	0.00	0.00
Valine	Val40	−2.14	0.36	−9.72	1.92
Isoleucine	Ile41	−10.25	1.74	0.00	0.00
Alanine	Ala42	−2.47	0.42	−16.94	3.34
Total energy		−588.77	—	−506.58	—

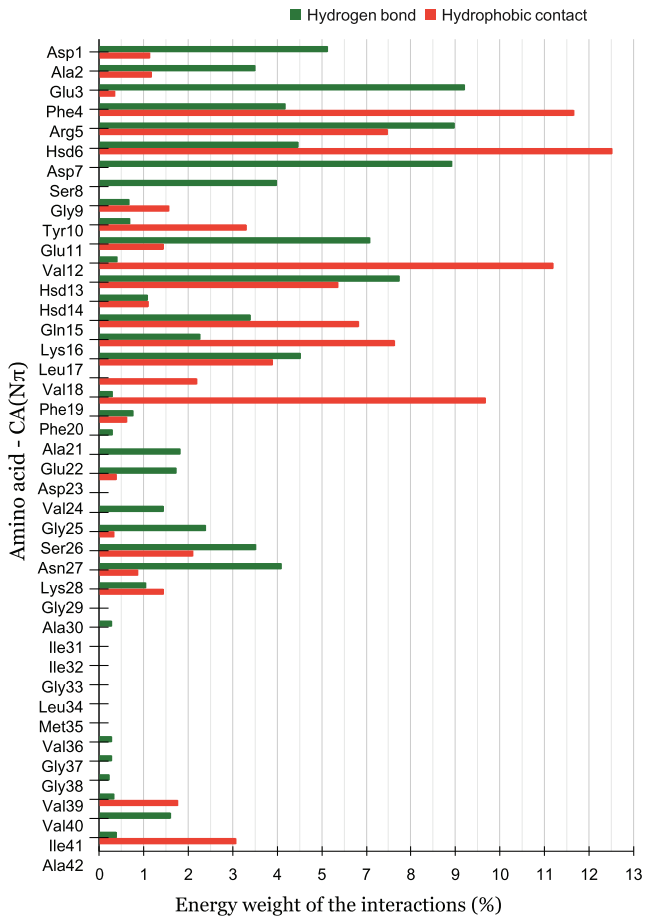

Fig. 7. (Color Online) Energy weight percentages for the amino acid interactions (hydrogen bonds and hydrophobic contacts) in the $CA_{N\pi}$/Aβ(1–42) complexes. We considered the 10 lowest energy complexes of 10 ligand/peptide conformations.

the previous results, the K_i values, presented in Table S2, have the same trend as that of the energies.

When it comes to the site of interaction of copper(II) with the peptide of Aβ(1–42), the results presented suggest that $CA_{N\pi}$ could interact with, at least, two of the amino acids responsible for complexation of the Aβ(1–42) peptide with the metal ion: The Hsd13 (by hydrogen bond) and Hsd6 (by hydrophobic contact). Energy weight percentages in Table 3 and Fig. 7 suggest that $CA_{N\pi}$ interacts through hydrogen bonds, mainly with the following amino acids: Glu3 (8.90%), Arg5 (8.65%), Asp7 (8.60%), Hsd13 (7.31%) and Glu11 (6.59%). By hydrophobic contact, the main interactions are Hsd6 (12.49%), Phe4 (11.57%), Val12 (11.05%), Phe19 (9.40%) and Lys16 (7.19%).

$CA_{N\pi}$ presents higher energy weight percentages with Hsd6 and Hsd13 (12.49% of interactions by hydrophobic contact and 7.31% of the hydrogen bond interactions, respectively) for Carnosines in their two

DOI: 10.1142/S2737416523500436
J. Comput. Biophys. Chem. **2023**, *22* (7), 829–843

tautomeric forms. In comparison, $CA_{N\tau}$ shows higher energy weight percentages with Asp1 (5.31% of hydrophobic contact interactions) and Hsd13 (8.70% of interactions by hydrogen bond and 5.41% by hydrophobic contact). Once the hydrogen bond interaction is stronger than the hydrophobic contact, $CA_{N\tau}$ tends to be more effective than $CA_{N\pi}$ in the steric impediment of the amino acids that participate in the complexation of copper(II). Moreover, according to the metallic hypothesis, this feature may be responsible for triggering the oligomerization of the Aβ(1–42) peptides.

3.3. Homocarnosines and Aβ interaction

We now turn to the results for the $HCA_{N\tau}/A\beta(1–42)_i$ interactions. Tables S6 and S7 in Supplementary Material present their related ΔG energies. As for the cases in the previous section, we considered the 10 lowest energy complexes of these ligand/peptide conformations. Table 4 and Fig. 8 present the energy weight results for the $HCA_{N\tau}/A\beta(1–42)_i$ interactions.

Similar to the case discussed in the previous section, the 10 lowest energies of each $HCA_{N\tau}/A\beta(1–42)$ complexes vary by 1 Kcal/mol, indicating that these complexes are equally likely. The complex with $A\beta(1–42)_1$ (with the lowest energy) differs by approximately 2 Kcal/mol than the complex with the $A\beta(1–42)_9$, 3 Kcal/mol when compared to the complexes with $A\beta(1–42)_2$ and $A\beta(1–42)_5$, and 4 Kcal/mol concerning complexes with $A\beta(1–42)_3$, $A\beta(1–42)_4$, $A\beta(1–42)_6$, $A\beta(1–42)_7$, $A\beta(1–42)_8$ and $A\beta(1–42)_{10}$. According to the previous results, the K_i values, presented in Table S3, have the same trend as the energies.

When it comes to the site of interaction of copper(II) with the peptide of Aβ(1–42), the results suggest that $HCA_{N\tau}$ could interact with at least three of the amino acids responsible for the complexation of the Aβ(1–42) peptide with the metal ion: Hsd13 and Asp1 (by hydrogen bond) and Hsd6 (by hydrophobic contact). From the results in Table 4 and Fig. 8, one can infer that $HCA_{N\tau}$ interacts by hydrogen bond mainly with the following amino acids: Gln15 (14.01%), Hsd13 (12.63%), Leu17 (12.40%), Asp1 (7.56%) and Arg5 (7.21%). By hydrophobic contact, the main interactions are Phe19 (22.41%), Phe4 (21.27%), Lys16 (14.83%), Val12 (12.91%), and Hsd6 (11.06%).

ΔG energy results for $HCA_{N\pi}/A\beta(1–42)_i$ interaction are shown in Supplementary Material (see Tables S8 and S9). From these results, the energy weights were calculated (hydrogen bond and hydrophobic contacts) and the results are presented in the Table 5 and Fig. 9.

Table 4. Energy weight percentages for each amino acid interaction (hydrogen bonds and hydrophobic contacts) in the $HCA_{N\tau}/A\beta(1–42)$ complexes obtained using molecular docking. We considered the 10 lowest energy complexes of 10 ligand/peptide conformations.

		Energy weight (Hydrogen bond)		Energy weight (Hydrophobic contact)	
Amino acid	Abbreviation	Kcal/mol	%	Kcal/mol	%
Aspartate	Asp1	–48.44	7.56	0.00	0.00
Alanine	Ala2	–16.11	2.51	0.00	0.00
Glutamate	Glu3	–37.76	5.89	0.00	0.00
Phenylalanine	Fene4	–22.29	3.48	–45.88	21.27
Arginine	Arg5	–46.25	7.21	–13.49	6.25
Histidine	Hsd6	–18.17	2.83	–23.85	11.06
Aspartate	Asp7	–36.01	5.62	0.00	0.00
Serine	Ser8	–14.86	2.32	0.00	0.00
Glycine	Gly9	–4.21	0.66	0.00	0.00
Tyrosine	Tyr10	–3.77	0.59	0.00	0.00
Glutamate	Glu11	–21.98	3.43	0.00	0.00
Valine	Val12	0.00	0.00	–27.84	12.91
Histidine	Hsd13	–80.98	12.63	–10.63	4.93
Histidine	Hsd14	–6.63	1.03	0.00	0.00
Glutamine	Gln15	–89.84	14.01	–2.79	1.29
Lysine	Lys16	–34.31	5.35	–31.98	14.83
Leucine	Leu17	–79.50	12.40	–9.36	4.34
Valine	Val18	–3.19	0.50	0.00	0.00
Phenylalanine	Phe19	–5.45	0.85	–48.33	22.41
Phenylalanine	Phe20	–9.17	1.43	0.00	0.00
Alanine	Ala21	–2.00	0.31	0.00	0.00
Glutamate	Glu22	0.00	0.00	0.00	0.00
Aspartate	Asp23	–2.00	0.31	0.00	0.00
Valine	Val24	0.00	0.00	0.00	0.00
Glycine	Gly25	–1.70	0.27	0.00	0.00
Serine	Ser26	–9.94	1.55	0.00	0.00
Asparagine	Asn27	–18.17	2.83	0.00	0.00
Lysine	Lys28	–8.83	1.38	0.00	0.00
Glycine	Gly29	–3.52	0.55	0.00	0.00
Alanine	Ala30	0.00	0.00	0.00	0.00
Isoleucine	Ile31	0.00	0.00	–1.52	0.70
Isoleucine	Ile32	0.00	0.00	0.00	0.00
Glycine	Gly33	0.00	0.00	0.00	0.00
Leucine	Leu34	0.00	0.00	0.00	0.00
Methionine	Met35	0.00	0.00	0.00	0.00
Valine	Val36	–1.83	0.29	0.00	0.00
Glycine	Gly37	–1.83	0.29	0.00	0.00
Glycine	Gly38	0.00	0.00	0.00	0.00
Valine	Val39	–3.51	0.55	0.00	0.00
Valine	Val40	–3.78	0.59	0.00	0.00
Isoleucine	Ile41	–3.20	0.50	0.00	0.00
Alanine	Ala42	–1.93	0.30	0.00	0.00
Total energy weight		–641.16	—	–215.67	—

DOI: 10.1142/S2737416523500436

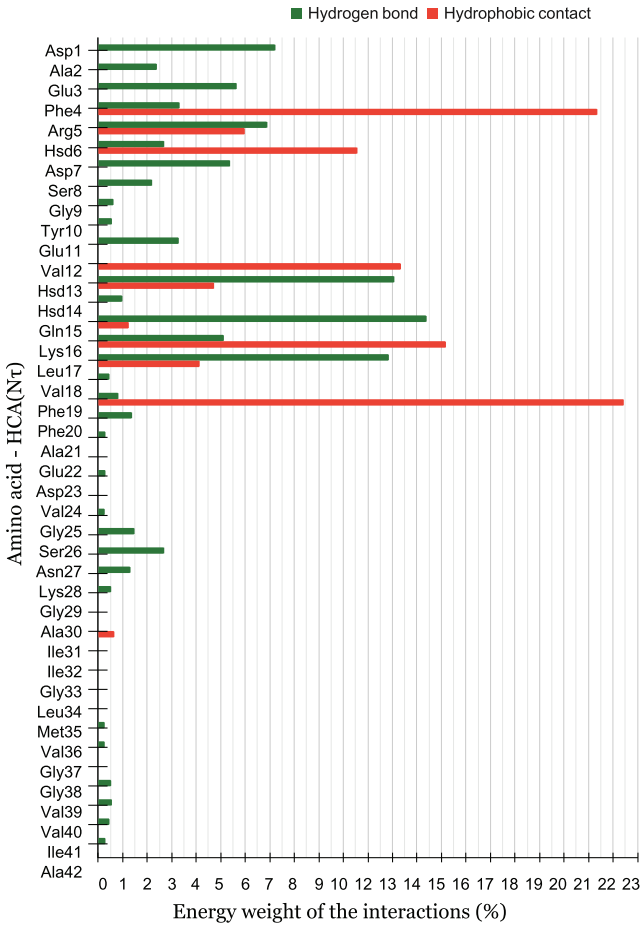

Fig. 8. (Color Online) Energy weight percentages for the amino acid interactions (hydrogen bonds and hydrophobic contacts) in the $HCA_{N\tau}$/Aβ(1–42) complexes. We considered the 10 lowest energy complexes of 10 ligand/peptide conformations.

The 10 lowest energies of each complex vary by approximately 1 kcal/mol, indicating that these complexes are equally likely. A$\beta(1–42)_1$ complex has the lowest energy and differs by about 1 Kcal/mol when compared to the A$\beta(1–42)_9$ complex, 2.5 Kcal/mol as contrasted with the A$\beta(1–42)_2$ and A$\beta(1–42)_5$ complexes, 3.0 Kcal/mol compared to the A$\beta(1–42)_3$, A$\beta(1–42)_7$, A$\beta(1–42)_8$ and A$\beta(1–42)_{10}$ complexes, and 3.5 Kcal/mol considering A$\beta(1–42)_4$ and A$\beta(1–42)_6$ complexes. Again, the K_i values, presented in Table S4, have the same trend as the energies.

For the site of interaction of copper(II) with Aβ(1–42), predicted by the literature,[16–19] the presented results suggest that $HCA_{N\pi}$ could interact with at least two of the amino acids responsible for the complexation of the Aβ(1–42) peptide with the metal ion: Hsd13 (by hydrogen bond and hydrophobic contact) and Hsd6 (by hydrophobic contact). The results in Table 5 and Fig. 9 indicate that $HCA_{N\pi}$ interacts by hydrogen bonds

Table 5. Energy weight percentages for each amino acid interaction (hydrogen bonds and hydrophobic contacts) in the $HCA_{N\tau}$/Aβ(1–42) complexes obtained using molecular docking. We considered the 10 lowest energy complexes of 10 ligand/peptide conformations.

		Energy weight (Hydrogen bond)		Energy weight (Hydrophobic contact)	
Amino acid	Abbreviation	Kcal/mol	%	Kcal/mol	%
Aspartate	Asp1	−28.15	4.44	0.00	0.00
Alanine	Ala2	−10.64	1.68	0.00	0.00
Glutamate	Glu3	−47.44	7.49	0.00	0.00
Phenylalanine	Fene4	−33.37	5.27	−56.81	26.63
Arginine	Arg5	−63.95	10.09	−17.73	8.31
Histidine	Hsd6	−24.31	3.84	−20.10	9.42
Aspartate	Asp7	−80.95	12.77	0.00	0.00
Serine	Ser8	−22.84	3.60	0.00	0.00
Glycine	Gly9	−16.57	2.61	0.00	0.00
Tyrosine	Tyr10	0.00	0.00	0.00	0.00
Glutamate	Glu11	−35.29	5.57	0.00	0.00
Valine	Val12	−2.51	0.40	−28.70	13.45
Histidine	Hsd13	−50.09	7.90	−23.96	11.23
Histidine	Hsd14	0.00	0.00	0.00	0.00
Glutamine	Gln15	−16.95	2.67	0.00	0.00
Lysine	Lys16	−41.99	6.63	−10.12	4.74
Leucine	Leu17	−27.98	4.41	−18.27	8.56
Valine	Val18	−2.08	0.33	−1.64	0.77
Phenylalanine	Phe19	−1.96	0.31	−35.99	16.87
Phenylalanine	Phe20	−8.01	1.26	0.00	0.00
Alanine	Ala21	−1.96	0.31	0.00	0.00
Glutamate	Glu22	−10.18	1.61	0.00	0.00
Aspartate	Asp23	−8.39	1.32	0.00	0.00
Valine	Val24	0.00	0.00	0.00	0.00
Glycine	Gly25	−2.68	0.42	0.00	0.00
Serine	Ser26	−12.76	2.01	0.00	0.00
Asparagine	Asn27	−23.23	3.67	0.00	0.00
Lysine	Lys28	−22.05	3.48	0.00	0.00
Glycine	Gly29	−13.93	2.20	0.00	0.00
Alanine	Ala30	−2.10	0.33	0.00	0.00
Isoleucine	Ile31	−2.26	0.36	0.00	0.00
Isoleucine	Ile32	0.00	0.00	0.00	0.00
Glycine	Gly33	0.00	0.00	0.00	0.00
Leucine	Leu34	0.00	0.00	0.00	0.00
Methionine	Met35	0.00	0.00	0.00	0.00
Valine	Val36	−1.66	0.26	0.00	0.00
Glycine	Gly37	−1.66	0.26	0.00	0.00
Glycine	Gly38	−2.10	0.33	0.00	0.00
Valine	Val39	0.00	0.00	0.00	0.00
Valine	Val40	−9.97	1.57	0.00	0.00
Isoleucine	Ile41	−3.76	0.59	0.00	0.00
Alanine	Ala42	0.00	0.00	0.00	0.00
Total energy weight		−633.77	—	−213.32	—

DOI: 10.1142/S2737416523500436
J. Comput. Biophys. Chem. **2023**, *22* (7), 829–843

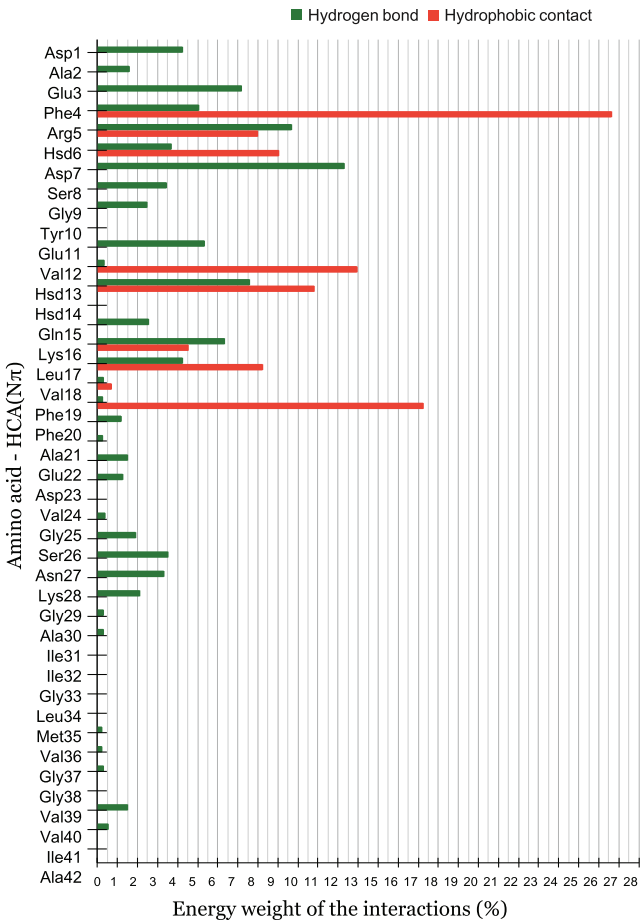

Fig. 9. (Color online) Energy weight percentages for the amino acid interactions (hydrogen bonds and hydrophobic contacts) in the $HCA_{N\pi}$/Aβ(1–42) complexes. We considered the 10 lowest energy complexes of 10 ligand/peptide conformations.

mainly with the following amino acids: Asp7 (12.77%), Arg5 (10.09%), Hsd13 (7.90%), Glu3 (7.4%) and Lys16 (6.63%). By hydrophobic contact, the main interactions are Phe4 (26.63%), Phe19 (16.87%), Val12 (13.45%), Hsd13 (11.23%) and Hsd6 (9.42%).

$HCA_{N\pi}$ has higher energy weight percentages with Hsd6 (9.42% of interactions by hydrophobic contact) and Hsd13 (7.90% of interactions by hydrogen bond and 11.23% of interactions by hydrophobic contact), in its two tautomeric forms. $HCA_{N\tau}$ has higher energy weight percentages with Asp1 (7.5% of interactions by hydrogen bond contact), Hsd6 (11.06% of hydrophobic by contact) and Hsd13 (12.63% of interactions by hydrogen bonds). In this sense, $HCA_{N\tau}$ is more effective than $HCA_{N\pi}$ in the steric impediment of the amino acids that participate in the complexation of the copper(II). Again, according to the metallic hypothesis, this interaction mechanism may be responsible for triggering the oligomerization of the Aβ(1–42) peptides.

Table 6. Interaction percentages (by hydrogen bond and hydrophobic contact) of the ligands/Aβ(1–42) for the main amino acids predicted to Aβ(1–42)/copper(II) complexation.

	Hyd	rogen	bond	Hydr	ophobic	contact
Complex	Asp1	Hsd6	Hsd13	Asp1	Hsd6	Hsd13
$CA_{N\tau}$/ Aβ(1–42)	5.31%	—	8.70%	—	—	5.41%
$CA_{N\pi}$/ Aβ(1–42)	—	—	7.31%	—	12.49%	—
$HCA_{N\tau}$/ Aβ(1–42)	7.56%	—	12.63%	—	11.6%	—
$HCA_{N\pi}$/ Aβ(1–42)	—	—	7.90%	—	9.42%	11.23%

Table 6 summarizes the main results of this case. Note that the main interactions (via hydrogen bonds) occurred with Hsd13, while Hsd6 interacts by hydrophobic contact. The CA and HCA interacted more often in the tautomeric form $N\tau$ through hydrogen bonds. The obtained values also indicate that $HCA_{N\tau}$ is the most effective ligand, i.e., the one with the highest percentage of interactions with the Aβ(1–42) peptide, considering that hydrogen bond interactions are stronger than hydrophobic contact interactions.

4. CONCLUSIONS

In summary, electronic structure calculations and molecular docking simulations were conducted to investigate the role of Carnosine and Homocarnosine natural compounds in order to prevent the progression of certain neurodegenerative diseases. The results revealed that these multi-target molecules can interact with at least two amino acids of the Aβ(1–42) peptide, which are responsible for the aggregation mediated by the metal ion Copper(II): Hsd13 through hydrogen bond and Hsd6 through hydrophobic contact. Moreover, the results demonstrated that Homocarnosine, in its tautomeric form N_τ, exhibited a higher number of hydrogen bond interactions with the Aβ(1–42) peptide, suggesting it may be more effective in the anti-aggregation process. These interactions can induce steric impediment, leading to a reduction in the rate of Aβ(1–42) peptide agglutination and oligomer formation, thereby preventing the formation of harmful protein deposits. In other words, these significant findings suggest that Carnosine and Homocarnosine molecules can act as antiaggregators, inhibiting the formation of amyloid plaques and ultimately stabilizing the progression of Alzheimer's disease and other neurodegenerative diseases.

DOI: 10.1142/S2737416523500436
J. Comput. Biophys. Chem. **2023**, *22* (7), 829–843

ACKNOWLEDGMENTS

The authors gratefully acknowledge the financial support from Brazilian research agen- cies CNPq, CAPES and FAP-DF. L. A. R. J acknowledge CENAPAD-SP, NACAD, and LNCC/MCTI for providing computational facilities.

CONFLICTS OF INTEREST

The authors confirm that there is no conflict of interest.

FUNDING INFORMATION

The authors gratefully acknowledge the financial support from Brazilian research agencies CNPq, CAPES, and FAP-DF. This study was financed in part by the Coordenação de Aperfeiçoamento de Pessoal de Nível Superior – Brazil (CAPES) – Finance Code 88887.691997/2022-00. R.G. and L.A.R.J acknowledge CENAPAD-SP for providing computational facilities.

References

1. Vos, T. *et al.* Global, Regional, and National Incidence, Prevalence, and Years Lived with Disability for 310 Diseases and Injuries, 1990–2015: A Systematic Analysis for the Global Burden of Disease Study 2015. *The Lancet* **2016**, *388* (10053), 1545–1602.
2. Reitz, C.; Brayne, C.; Mayeux, R. Epidemiology of Alzheimer Disease. *Nat. Rev. Neurol.* **2011**, *7* (3), 137.
3. Serrano-Pozo, A.; Frosch, M. P.; Masliah, E.; Hyman, B. T. Neuropathological Alterations in Alzheimer Disease. *Cold Spring Harbor Perspect. Med.* **2011**, *1* (1), a006189.
4. Evans, D. A.; Harris Funkenstein, H.; Albert, M. S.; Scherr, P. A.; Cook, N. R.; Chown, M. J.; Hebert, L. E.; Hennekens, C. H.; Taylor, J. O. Prevalence of Alzheimer's Disease in a Community Population of Older Persons: Higher Than Previously Reported. *JAMA* **1989**, *262* (18), 2551–2556.
5. Hebert, L. E.; Scherr, P. A.; Beckett, L. A.; Albert, M. S.; Pilgrim, D. M.; Chown, M. J.; Funkenstein, H. H.; Evans, D. A. Age-Specific Incidence of Alzheimer's Disease in a Community Population. *JAMA* **1995**, *273* (17), 1354–1359.
6. Small, G. W.; Rabins, P. V.; Barry, P. P.; Buckholtz, N. S.; DeKosky, S. T.; Ferris, S. H.; Finkel, S. I.; Gwyther, L. P.; Khacha- turian, Z. S.; Lebowitz, B. D.; McRae, T. D.; Morris, J. C.; Oakley, F.; Schneider, L. S.; Streim, J. E.; Sunderland, T.; Teri, L. A.; Tune, L. E. Diagnosis and Treatment of Alzheimer Disease and Related Disorders: Consensus Statement of the American Association for Geriatric Psychiatry, the Alzheimer's Association, and the American Geriatrics Society. *JAMA* **1997**, *278* (16), 1363–1371.
7. Forlenza, O. V. Transtornos depressivos na doen¸ca de alzheimer: Diagnóstico e tratamento. *Braz. J. Psychiatry* **2000**, 22, 87–95.
8. Francis, P. V.; Palmer, A. M.; Snape, M.; Wilcock, G. K. The Cholinergic Hypothesis of Alzheimer's Disease: A Review of Progress. *J. Neu rol. Neurosurg. Psychiatry* **1999**, *66* (2), 137–147.
9. Hardy, J. A.; Higgins, G. A. Alzheimer's Disease: The Amyloid Cascade Hypothesis. *Science* **1992**, *256* (5054), 184–186.
10. Maccioni, R. B.; Farías, G.; Morales, I.; Navarrete, L. The Revitalized Tau Hypothesis on Alzheimer's Disease. *Arch. Med. Res.* **2010**, *41* (3), 226–231.
11. de la Monte, S. M.; Wands, J. R. Alzheimer's Disease is Type 3 Diabetes — Evidence Reviewed. *J. Diabetes Sci. Technol.* **2008**, *2* (6), 1101–1113, PMID: 19885299.
12. Bush, A. I.; Tanzi, R. E. Therapeutics for Alzheimer's Disease Based on the Metal Hypothesis. *Neurotherapeutics* **2008**, *5* (3), 421–432.
13. Lovell, M. A.; Robertson, J. D.; Teesdale, W. J.; Campbell, J. L.; Markesbery, W. R. Copper, Iron and Zinc in Alzheimer's Disease Senile Plaques. *J. Neurol. Sci.* **1998**, *158* (1), 47–52.
14. Kozlowski, H.; Luczkowski, M.; Remelli, M.; Valensin, D. Copper, Zinc and Iron in Neurodegenerative Diseases (Alzheimer's, Parkinson's and Prion Diseases). *Coord. Chem. Rev.* **2012**, *256* (19), 2129–2141.
15. Maynard, C. J.; Cappai, R.; Volitakis, I.; Cherny, R. A.; White, A. R.; Beyreuther, K.; Masters, C. L.; Bush, A. I.; Li, Q.-X. Over-Expression of Alzheimer's Disease Amyloid-β Opposes the Age-Dependent Elevations of Brain Copper and Iron. *J. Biol. Chem.* **2002**, *277* (47), 44670–44676.
16. Drew, S. C.; Masters, C. L.; Barnham, K. J. Alanine-2 Carbonyl is an Oxygen Ligand in $Cu2^{+}$ Coordination of Alzheimer's Disease Amyloid-*B* Peptide — Relevance to n-Terminally Truncated Forms. *J. Am. Chem. Soc.* **2009**, *131* (25), 8760–8761.
17. Faller, P.; Hureau, C. Bioinorganic Chemistry of Copper and Zinc Ions Coordinated to Amyloid-β Peptide. *Dalton Trans.* **2009**, *7*, 1080–1094.
18. Faller, P.; Hureau, C.; Berthoumieu, O. Role of Metal Ions in the Self-Assembly of the Alzheimer's Amyloid-β Peptide. *Inorg. Chem.* 2013, *52* (21), 12193–12206.
19. Huy, P. D. Q.; Vuong, Q. V.; Penna, G. L.; Faller, P.; Li, M. L. Impact of Cu(ii) Binding on Structures and Dynamics of aβ42 Monomer and Dimer: Molecular Dynamics Study. *ACS Chem. Neurosci.* **2016**, *7* (10), 1348–1363.

20. Faller, P.; Hureau, C.; La Penna, G. Metal Ions and intrinsically Disordered Proteins and Peptides: From Cu/Zn Amyloid-β to General Principles. *Acc. Chem. Res*. **2014**, *47* (8), 2252–2259.
21. Hureau, C. Coordination of Redox Active Metal Ions to the Amyloid Precursor Protein and to Amyloid-β Peptides involved in Alzheimer Disease. Part 1: An Overview. *Coord. Chem. Rev*. **2012**, *256* (19–20), 2164–2174.
22. Ghodsi, R.; Kheirouri, S. Carnosine and Advanced Glycation End Products: A Systematic Review. *Amino Acids* **2018**, *50* (9), 1177–1186.
23. Chmielewska, K.; Dzierzbicka, K.; Inkielewicz-Stepniak, I.; Przybylowska, M. Therapeutic Potential of Carnosine and its Derivatives in the Treatment of Human Diseases. *Chem. Res. Toxicol*. **2020**, *33* (7), 1561–1578.
24. Prokopieva, V. D.; Yarygina, E. G.; Bokhan, N. A.; Ivanova, S. A. Use of Carnosine for Oxidative Stress Reduction in Different Pathologies. *Oxid. Med. Cell. Longev*. **2016**, 2016, 2939087.
25. Boldyrev, A. A.; Aldini, G.; Derave, W. Physiology and Patho-Physiology of Carnosine. *Physiol. Rev*. **2013**; *93* (4), 1803–1845.
26. Hipkiss, A. R. Would Carnosine or a Carnivorous Diet Help Suppress Aging and Associated Pathologies? *Ann. New York Acad. Sci*. **2006**, *1067* (1), 369–374.
27. Hipkiss, A. R. Carnosine, A Protective, Anti-Ageing Peptide? *Int. J. Biochem. Cell Biol*. **1998**, *30* (8), 863–868.
28. Begum, G.; Cunliffe, A.; Leveritt, M. Physiological Role of Carnosine in Contracting Muscle. *Int. J. Sport Nutr. Exerc. Metab*. **2005**, *15* (5), 493–514.
29. Bate Smith, E. C. The Buffering of Muscle in Rigor; Protein, Phosphate and Carnosine. *J. Physiol*. **1938**, *92* (3), 336.
30. Kawahara, M.; Tanaka, K.; Kato-Negishi, M. Zinc, Carnosine, and Neurodegenerative Diseases. *Nutrients* **2018**, *10* (2), 147.
31. Dobbie, H.; Kermack, W. O. Complex-Formation Between Polypeptides and Metals. 2. The Reaction Between Cupric Ions and Some Dipeptides. *Biochem. J*. **1955**, *59* (2), 246.
32. Bruce Martin, R.; Edsall, J. T. The Association of Divalent Cations with Acylated Histidine Derivatives1. *J. Am. Chem. Soc*. **1960**, *82* (5), 1107–1111.
33. Freeman, H. C.; Szymanski, J. T. Crystallographic Studies of Metal–Peptide Complexes. v.(β-alanyl-l-histidinato) Copper (ii) Dihydrate. *Acta Crystallograph*. **1967**, *22* (3), 406–417.
34. Bersohn, R.; Ihnat, M. E. Proton Nuclear Magnetic Resonance Study of the Copper (ii)-Carnosine Complex in Aqueous Solution. *Biochemistry* **1970**, *9* (23), 4555–4566.
35. Matsukura, T.; Takahashi, T.; Nishimura, Y.; Ohtani, T.; Sawada, M.; Shibata, K. Characterization of Crystalline l-Carnosine zn (ii) Complex (z-103), A Novel Anti-Gastric Ulcer Agent: Tautomeric Change of Imidazole Moiety upon Complexation. *Chem. Pharm. Bull*. **1990**, *38* (11), 3140–3146.
36. Trouillas, P.; Marsal, P.; Siri, D.; Lazzaroni, R.; Duroux, J.-L. A Dft Study of the Reactivity of Oh Groups in Quercetin and Taxifolin Antiox-idants: The Specificity of the 3-Oh Site. *Food Chem*. **2006**, *97* (4), 679–688.
37. Wu, Q.; Su, H.; Wang, H.; Wang, H. Ab Initio Calculations, Structure, NBO and NCI Analyses of X–H π Interactions. *Chem. Phys. Lett*. **2018**, *693*, 202–209.
38. Mohammadi, M. D.; Abdullah, H. W. Ab Initio Investigation for the Adsorption of Acrolein onto the Surface of C60, C59Si, and C59 Ge: NBO, QTAIM, and NCI Analyses. *Struct. Chem*. **2022**, *33* (3), 1–16.
39. Savoo, N.; Malan, F. P.; Rhyman, L.; Ramasami, P. Molecular Insights of Metal–Metal Interactions in Transition Metal Complexes Using Computational Methods. *Pure Appl. Chem*. **2021**, *93* (5), 579–589.
40. Boto, R. A.; Peccati, F.; Laplaza, R.; Quan, C.; Carbone, A.; Piquemal, J.-P.; Maday, Y.; Contreras-Garcia, J. Nciplot4: Fast, Robust, and Quantitative Analysis of Noncovalent Interactions. *J. Chem. Theory Comput*. **2020**, *16* (7), 4150–4158.
41. Johnson, E. R.; Keinan, S.; Mori-Sánchez, P.; Contreras-García, J.; Cohen, A. J.; Yang, W. Revealing Noncovalent Interactions. *J. Am. Chem. Soc*. **2010**, *132* (18), 6498–6506.
42. Contreras-García, J.; Johnson, E. R.; Keinan, S.; Chaudret, R.; Piquemal, J.-P.; Beratan, D. N.; Yang, W. Nciplot: A Program for Plotting Noncovalent Interaction Regions. *J. Chem. Theory Comput*. **2011**, *7* (3), 625–632.
43. D'Avila Braga Sette, C. Reconhecimento molecular dos compostos natu- rais cinamaldeído, curcumina e ácido rosmarínico pelo peptídeo β-amilóide(1-42). Doutorado, Universidade de Brasília, Distrito Federal, 2020.
44. Morris, G. M.; Goodsell, D. S.; Huey, R.; Hart, W. E.; Halliday, S.; Belew, R.; Olson, A. J., AutoDock4 and AutoDockTools4: Automated docking with selective receptor flexibility. *J. Comput. Chem*. **2009**, *30* (16), 2785–2791.
45. Gasteiger, J.; Marsili, M. Iterative Partial Equalization of Orbital Electronegativity — A Rapid Access to Atomic Charges. *Tetrahedron* **1980**, *36* (22), 3219–3228.
46. Morris, G. M.; Goodsell, D. S.; Halliday, R. S.; Huey, R.; Hart, W. E.; Belew, R. K.; Olson, A. J. Automated Docking using a Lamarckian Genetic Algorithm and an Empirical Binding Free Energy Function. *J. Comput. Chem*. **1998**, *19* (14), 1639–1662.
47. Laskowski, R. A.; Swindells, M. B. Ligplot+: Multiple Ligand–Protein Interaction Diagrams for Drug Discovery. *J. Chem. Inf. Model*. **2011**, *51* (10), 2778–2786, PMID: 21919503.

48. Chandler, D. Interfaces and the Driving Force of Hydrophobic Assembly. *Nature* **2005**, *437* (7059), 640–647.
49. McDonald, I. K.; Thornton, J. M. Satisfying Hydrogen Bonding Potential in Proteins. *J. Mol. Biol.* **1994**, *238* (5), 777–793.
50. Dobbie, H.; Kermack, W. O. Complex-Formation between Polypeptides and Metals. 2. The Reaction between Cupric Ions and Some Dipeptides. *Biochem. J.* **1955**, *59* (2), 246–257.
51. Matsukura, T.; Takahashi, T.; Nishimra, Y.; Ohtani, T.; Sawada, M.; Shibata, K. Characterization of Crystalline l-Carnosine zn(ii) Complex (z-103), A Novel Anti-Gastric Ulcer Agent: Tautomeric Change of Imida- Zole Moiety upon Complexation. *Chem. Pharm. Bull.* **1990**, *38* (11), 3140–3146.

DOI: 10.1142/S2737416523500436
J. Comput. Biophys. Chem. **2023**, *22* (7), 829–843